A comparison between analytic and numerical methods for modelling automotive dissipative silencers with mean flow

R. Kirby *

School of Engineering and Design, Mechanical Engineering, Brunel University, Uxbridge, Middlesex UB8 3PH, UK

ARTICLE INFO

ABSTRACT

Identifying an appropriate method for modelling automotive dissipative silencers normally requires one to choose between analytic and numerical methods. It is common in the literature to justify the choice of an analytic method based on the assumption that equivalent numerical techniques are more computationally expensive. The validity of this assumption is investigated here, and the relative speed and accuracy of two analytic methods are compared to two numerical methods for a uniform dissipative silencer that contains a bulk reacting porous material separated from a mean gas flow by a perforated pipe. The numerical methods are developed here with a view to speeding up transmission loss computation, and are based on a mode matching scheme and a hybrid finite element method. The results presented demonstrate excellent agreement between the analytic and numerical models provided a sufficient number of propagating acoustic modes are retained. However, the numerical mode matching method is shown to be the fastest method, significantly outperforming an equivalent analytic technique. Moreover, the hybrid finite element method is demonstrated to be as fast as the analytic technique. Accordingly, both numerical techniques deliver fast and accurate predictions and are capable of outperforming equivalent analytic methods for automotive dissipative silencers.

1. Introduction

Numerous models are now available for computing sound attenuation by dissipative silencers typically found on internal combustion engines. The models developed range from simple plane wave analytic models to fully three-dimensional numerical models. The computational effort required by each method can vary significantly and one is usually left with a decision of how best to balance computational speed with solution accuracy. This article aims to develop a better understanding of how different approaches compare in terms of speed and accuracy by analysing four different methodologies: (i) an analytic model based on the fundamental mode only; (ii) an analytic mode matching method; (iii) a numerical mode matching method; and (iv) a hybrid numerical method. Here, the two numerical methods presented are modifications of existing techniques with a view to improving computational efficiency without sacrificing accuracy. The accuracy and efficiency of each method is then compared for a straight through dissipative silencer containing a perforated pipe separating a mean fluid flow from a bulk reacting porous material.

The most straightforward and computationally efficient approach to modelling automotive dissipative silencers is to assume that only the fundamental mode propagates within each silencer section. This allows for a simple closed form

* Corresponding author. Tel.: +44 1895 266687; fax: +44 1895 256392.
  E-mail address: ray.kirby@brunel.ac.uk

analytic solution to be written, see Peat [1] and, later, Kirby [2]. This method is attractive since one does not need to find roots of a governing eigenequation and so the method is very quick. There is, however, a penalty to pay for this speed and Kirby [2] demonstrates that at higher frequencies and for larger silencers the method lacks accuracy. Nevertheless, the methodology is useful for low frequency design work and, since it includes both mean flow and a perforated pipe, Kirby's method [2] will be reviewed later on.

To improve prediction accuracy it is necessary to include higher order modes, at least within the silencer section. This complicates matters since one must now solve the governing eigenequation for the silencer section, which is far from straightforward when mean flow is present. This normally requires an iterative method such as, for example, the Newton–Raphson method [3–5] or the Secant method [6,7]. The different iterative methods have their relative advantages and disadvantages, but the very fact that iterative solutions are required impacts on computational efficiency. On solving the governing eigenequation it is necessary to match axial continuity conditions over the inlet and outlet planes of the silencer. When no mean flow is present analytic methods have been used to enforce continuity of pressure and axial velocity with little difficulty [3,4,6–8], even for multiple area discontinuities [9] and for large silencers [10]. However, when mean flow is present Kirby and Denia [5] suggested that it is necessary to change the axial continuity conditions so that they equate to the transverse continuity conditions used to match between the mean flow region and the absorbing material. Analytic mode matching then delivers a transfer matrix for the silencer in which normally between four and eight silencer modes need to be included [3,5] in order to obtain sufficient accuracy and so inverting the transfer matrix is normally very quick. It is tempting then to view analytic mode matching as very computationally efficient and much faster than numerical methods; however, the speed of analytic mode matching schemes depends almost entirely on the time taken to find the roots of the governing eigenequation, and it is not necessarily the case that this is faster than equivalent numerical methods. This issue was noted by Albelda et al. [8], who avoided solving the usual dispersion relation by sub-dividing the silencer cross-section in order to find two sets of modes after first enforcing zero pressure and zero radial velocity over the perforated pipe. The authors note that these two sets of modes may be computed analytically for circular and elliptical geometries, although they do not provide details of the dispersion relations that follow. The Galerkin method is then used to find the eigenvectors and axial wavenumbers for the silencer itself, and for circular and elliptical geometries the integrals that follow may be calculated analytically. The usual mode matching procedure is then employed to find the silencer transmission loss. Accordingly, this method neatly sidesteps the root finding problems associated with the more usual silencer eigenequation and so is potentially faster than the traditional analytical methods. Furthermore, an extension of this method to include mean flow and a perforated pipe has recently been reported [11], although the full details have yet to be published.

Numerical methods generally separate into two different approaches: those which take advantage of the uniform geometry often present in automotive silencers, and those which seek to model the whole silencer chamber. The first approach clearly has the potential to speed up solutions although, in common with analytic mode matching, this method can be cumbersome if many different discontinuities are present such as inlet and outlet extensions. Conversely, the second approach is traditionally thought to be very time consuming and this method appears to be more suited to very complex non-uniform silencer designs. Accordingly, for a uniform dissipative silencer a numerical mode matching method appears to be the most attractive, and this has the added advantage of avoiding an iterative technique to solve the governing eigenequation. For example, Astley et al. [12] use the finite element method to solve the governing eigenequation and then use collocation to match across a discontinuity in a lined rectangular duct. Later, Glav [13,14] used a point matching technique to study uniform silencers with irregular cross-sections, although the rate of convergence of this method is sensitive to silencer geometry and the collocation grid chosen. Kirby [15] extended the work of Astley et al. [12] and applied collocation to silencers of elliptical cross-section containing both mean flow and a perforated pipe. This represents a general method for silencers of arbitrary cross-section; however, because the method is numerically based it has generally been viewed as computationally inefficient for circular silencers and inherently slower than equivalent analytic techniques.

General numerical schemes suitable for complex silencer geometries have also been applied in the study of automotive silencers, see for example Bilawchuk and Fyfe [16] who review the application of the finite element method (FEM) and the boundary element method (BEM). When no mean flow is present, the BEM has been applied successfully to complicated silencers geometries [16–18]. Similarly, the FEM has also been used to study dissipative silencers without flow [16,19], and Mehdizadeh and Paraschivoiu [20] report a comprehensive three-dimensional approach. Clearly, using a fully three-dimensional model is very computationally expensive and the number of degrees of freedom used by Mehdizadeh and Paraschivoiu [20] appears to be excessive, at least for a uniform circular silencer. It is noticeable, however, that the boundary element models do not combine the effects of both mean flow and a perforated pipe, and only Peat and Rathi [21] have successfully added mean flow to a finite element model of a bulk reacting dissipative silencer. Here, Peat and Rathi focus on computing the silencer four poles, which requires solving the problem twice. Thus, if one desires only the silencer transmission loss then this method is more computationally expensive than, say, the three point method [20], although computation of the silencer four poles does allow predictions to be easily incorporated into models of an overall silencer system. Peat and Rathi [21] also omitted a perforated pipe, but superimposed a mean bias flow inside the absorbing material in order to examine the effect this has on silencer performance. It is likely, however, that a perforated pipe will lower the mean flow inside the porous material and so it appears justified to neglect this effect, especially as perforated pipes are always present in commercial silencers. Peat and Rathi [21] demonstrated generally good agreement

with the analytic mode matching method of Cummings and Chang [3], at least at higher frequencies, although it appears here to be reasonable to assume that the FEM should be slower than the analytic mode matching method for comparable accuracy.

The relative computational efficiency and accuracy of predictions for two analytic and two numerical methods are reviewed here. This is carried out for a circular dissipative silencer containing mean flow and a perforated pipe. Here, particular attention will be paid to improving existing numerical techniques so that they are more computationally efficient for a given degree of accuracy. The analytic techniques to be used as benchmark predictions are the low frequency algorithm of Kirby [2], which will be abbreviated here as the APW method, and the analytic mode matching method of Kirby and Denia [5], abbreviated as the AMM method. The analytic method of Kirby and Denia has been chosen here as it represents the more usual mode matching approach (see also Refs. [3,4,6,7]), and in the absence of further details on the method of Albelda et al. [11]. The analytic methods are compared against new versions of the point collocation method of Kirby [15] and the FEM of Peat and Rathi [21]. Here, the point collocation method (abbreviated as the NMM method) is modified by including the new axial matching conditions reported by Kirby and Denia [5] and enforcing these conditions using mode matching rather than collocation. The FEM of Peat and Rathi [21] is modified to include a perforated pipe, but the method will also be improved by utilising the hybrid numerical method recently reported by Kirby [22]. This hybrid numerical method is not new (see for example Ref. [23]), but it has yet to be applied to the study of dissipative silencers, with or without mean flow. The hybrid method uses a modal representation for the sound field in the inlet and outlet pipes and, using mode matching, "joins" this to a finite element representation of the sound field in the silencer chamber. This avoids the need to mesh the inlet and outlet pipes, but also avoids the rather cumbersome three point method for finding silencer transmission loss and so makes it very straightforward to find the silencer four poles. Accordingly, the hybrid method (abbreviated here as the HFE method) has the potential to speed up the FEM for dissipative silencers and the efficiency of this method will be benchmarked against the other analytic and numerical methodologies. The article begins by reviewing the essential elements of the analytic models. A detailed description of the two numerical models is then reported and results are presented in the form of transmission loss predictions; the analysis that follows will focus on the relative efficiency of each method rather than a direct comparison with experimental data (which has been reported elsewhere).

2. Theory

The automotive dissipative silencer is assumed to consist of a region of (isotropic) bulk reacting porous material of arbitrary cross-section, separated by a concentric perforated pipe from a central airway that contains a uniform mean gas flow of Mach number M, see Fig. 1. The inlet and outlet pipe walls, and the walls of the silencer chamber, are assumed to be rigid and impervious to sound. Before reviewing different numerical and analytic methods for analysing this problem the general governing equations, boundary conditions, and expressions for the inlet and outlet pipes are reported. Accordingly, the acoustic wave equation for region q ($q = 1,2,3$ or 4) is given by

$$\frac{1}{c_q^2}\frac{D^2 p_q'}{Dt^2} - \nabla^2 p_q' = 0, \tag{1}$$

where c_q is the speed of sound, p_q' is the acoustic pressure, and t is time. The hard wall boundary condition is given by

$$\nabla p_q' \cdot \mathbf{n}_q = 0, \tag{2}$$

over the outer surface Γ_w, where $\mathbf{n}_q$ is the outward unit normal vector in region q. A modal representation for the sound field in regions R_1 and R_4 is used in each of the methods that follow and so the sound pressure is written as an expansion
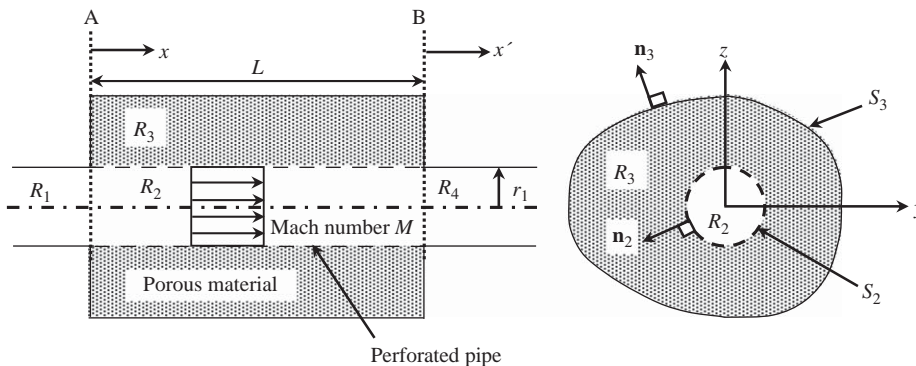

Fig. 1. Geometry of silencer.

over the pipe eigenmodes, to give

$$p_1'(x,y,z) = \sum_{n=0}^{\infty} F^n \Phi_i^n(y,z) e^{-ik_0\lambda_i^n x} + \sum_{n=0}^{\infty} A^n \Phi_r^n(y,z) e^{-ik_0\lambda_r^n x}, \tag{3}$$

and

$$p_4'(x',y,z) = \sum_{n=0}^{\infty} D^n \Phi_i^n(y,z) e^{-ik_0\lambda_i^n x'} + \sum_{n=0}^{\infty} E^n \Phi_r^n(y,z) e^{-ik_0\lambda_r^n x'}. \tag{4}$$

Here, F^n, A^n, D^n and E^n are the modal amplitudes; λ_i^n are the incident and λ_r^n the reflected axial wavenumbers, and Φ_i^n are the incident and Φ_r^n the reflected eigenfunctions in regions 1 and 4, respectively. A time dependence of $e^{i\omega t}$ is assumed (where $i = \sqrt{-1}$ and ω is the radian frequency) and $k_0 = \omega/c_0$, where c_0 is the isentropic speed of sound in air. For a circular pipe with acoustically hard walls, the wavenumbers and eigenfunctions may easily be found (see Ref. [5]).

For the silencer chamber, region R_c ($= R_2+R_3$), different methods will be used to find the sound pressure distribution; however, regions R_2 and R_3 will be "joined" using the same radial boundary conditions over the perforated pipe. Following Kirby and Denia [5] this yields

$$\mathbf{u}_2 \cdot \mathbf{n}_2 = -\left[1 - i\frac{M}{k_0}\frac{\partial}{\partial x}\right]^{Q-1} \mathbf{u}_3 \cdot \mathbf{n}_3, \tag{5}$$

and

$$p_2' - p_3' = \rho_0 c_0 \zeta \mathbf{u}_3 \cdot \mathbf{n}_3. \tag{6}$$

Here, the fluid density in region R_2 is ρ_0, the acoustic velocity vector in region q is denoted by $\mathbf{u}_q$, and the (dimensionless) impedance of the perforated pipe is denoted by ζ. In view of the discussions by Kirby and Denia [5] on the measurement of the impedance of the perforated pipe, the constant Q (where $1 \leqslant Q \leqslant 2$) is introduced here so that $Q = 1$ corresponds to continuity of velocity, and $Q = 2$ to continuity of displacement.

2.1. Analytic methods

Two different analytic methodologies are reviewed here, the plane wave (APM) method of Kirby [2] and the mode matching (AMM) method of Kirby and Denia [5]. Both restrict their analysis to circular dissipative silencers. Of course, these methods may in principle be extended to other regular geometries provided suitable transverse analytic functions are available, see for example the Mathieu functions used for elliptical silencers by Denia et al. [24]. As both analytic methods have been reported elsewhere only a brief review of the methodology behind each approach will be included here. Both analytic methods depend on using a modal representation of the sound fields in each region and then matching appropriate continuity conditions over the silencer inlet and outlet planes (planes A and B, respectively). Here, the AMM method uses a closed form analytic solution that calculates the fundamental modes only, whereas the NMM method uses the Newton–Raphson method to locate higher order modes [5]. In fact, it is in locating higher order modes that difficulties with analytic methods arise, as an iterative method is required in order to find the roots of the eigenequation. Kirby and Denia [5] note that when mean flow is present locating all required roots is not always straightforward and this can lead to analytic methods taking longer to run than one would normally expect. On locating the desired higher order modes, the axial continuity conditions are enforced, although for fundamental mode propagation these equations reduce to continuity of volume velocity and pressure [2]. When higher order modes are present Kirby and Denia [5] proposed using continuity of pressure and displacement, although the kinematic condition was written generally so that modifications may be made in light of further experimental evidence. On applying the matching conditions it is then straightforward to construct a matrix for the silencer and, after application of the inlet and outlet axial boundary conditions, this is solved for the modal amplitudes. The overall performance of the silencer is readily obtained from the modal amplitudes, which is normally quantified in terms of the silencer transmission loss (TL). Kirby and Denia [5] also reported expressions for the four poles of the dissipative silencer; however, these expressions are incorrect and a corrected methodology will be introduced in Section 2.2.1. For the multi-mode method, the bulk of the solution time is taken up in finding the roots of the governing eigenequation and this will be reviewed in Section 3. Once this has been done, finding the modal amplitudes does not normally take very long since the matrix that must be inverted is usually small, assuming that a relatively small number of modes is retained in the silencer chamber (normally between six and 10).

2.2. Numerical mode matching

A numerical matching technique is included here because it is suitable for analysing silencers of arbitrary but uniform cross-section, but also for circular silencers it avoids root finding algorithms such as the Newton–Raphson method. A point collocation scheme was reported by Kirby [15] for elliptical silencers and this method forms the basis of the numerical matching scheme that follows. However, instead of matching over discrete collocation points on the silencer cross-section, the method presented here will use numerical mode matching and so numerical integration is used to enforce the axial

matching conditions over planes A and B. Here, the numerical mode matching (NMM) method adopts a modal representation for the sound field in the inlet and outlet pipes given by Eqs. (3) and (4); similarly for the silencer section

$$p'_c(x,y,z) = \sum_{n=0}^{\infty} B^n \Psi_i^n(y,z)e^{-ik_0 k_i^n x} + \sum_{n=0}^{\infty} C^n \Psi_r^n(y,z)e^{-ik_0 k_r^n x}. \tag{7}$$

Here, B^n and C^n are the modal amplitudes, k_i^n are the incident and k_r^n the reflected axial wavenumbers, and Ψ_i^n are the incident and Ψ_r^n the reflected eigenfunctions. To construct the governing eigenequation for the silencer chamber, the radial boundary conditions defined by Eqs. (5) and (6) are used, along with the assumption that the acoustic velocity normal to the walls of the silencer is zero. The eigenproblem is then solved using the finite element method, and so the eigenvector for region R_c is approximated as

$$\Psi(y,z) = \sum_{j=1}^{n_s} N_j(y,z)\Psi_{s_j}, \tag{8}$$

where N_j is a global trial (or shape) function for the (transverse) finite element mesh, Ψ_{s_j} is the value of $\Psi(y,z)$ at node j, and n_s is the number of nodes (or degrees of freedom) lying on the silencer cross section in region R_c. Expressing Eq. (8) in vector form yields

$$\Psi(y,z) = [N_1(y,z), N_2(y,z), \ldots, N_{n_s}(y,z)] \begin{bmatrix} \Psi_{s_1} \\ \Psi_{s_2} \\ \Psi_{s_{n_s}} \end{bmatrix} = \mathbf{N}\boldsymbol{\Psi}. \tag{9}$$

Following Kirby [15], the governing eigenequation is written as

$$\begin{bmatrix} \mathbf{0} & \mathbf{I} \\ -\mathbf{R}_3^{-1}\mathbf{R}_1 & -\mathbf{R}_3^{-1}\mathbf{R}_2 \end{bmatrix} \begin{Bmatrix} \boldsymbol{\Psi} \\ k\boldsymbol{\Psi} \end{Bmatrix} = k \begin{Bmatrix} \boldsymbol{\Psi} \\ k\boldsymbol{\Psi} \end{Bmatrix}, \tag{10}$$

where $\mathbf{I}$ is an identity matrix. The matrices $\mathbf{R}_1$, $\mathbf{R}_2$ and $\mathbf{R}_3$ are given by

$$\mathbf{R}_1 \mathbf{p}_s = [\mathbf{H}_2 - k_0^2 \mathbf{L}_2]\boldsymbol{\Psi}_2 + \tilde{\rho}^{-1}[\mathbf{H}_3 + \Gamma^2 \mathbf{L}_3]\boldsymbol{\Psi}_3 + (ik_0/\zeta)[\mathbf{L}_{p_3} - \mathbf{L}_{p_2}]\{\boldsymbol{\Psi}_{p_3} - \boldsymbol{\Psi}_{p_2}\}, \tag{11}$$

$$\mathbf{R}_2 \mathbf{p}_s = 2Mk_0^2 \mathbf{H}_2 \boldsymbol{\Psi}_2 + Q(ik_0 M/\zeta)\mathbf{L}_{p_2}\{\boldsymbol{\Psi}_{p_3} - \boldsymbol{\Psi}_{p_2}\}, \tag{12}$$

$$\mathbf{R}_3 \mathbf{p}_s = k_0^2(1 - M^2)\mathbf{H}_2 \boldsymbol{\Psi}_2 + \tilde{\rho}^{-1}k_0^2 \mathbf{H}_3 \boldsymbol{\Psi}_3 - (Q-1)(ik_0 M^2/\zeta)\mathbf{L}_{p_2}\{\boldsymbol{\Psi}_{p_3} - \boldsymbol{\Psi}_{p_2}\}. \tag{13}$$

In addition,

$$\mathbf{H}_2 = \int_{R_2} \nabla \mathbf{N}^T \cdot \nabla \mathbf{N} \, dy \, dz, \tag{14}$$

$$\mathbf{H}_3 = \int_{R_3} \nabla \mathbf{N}^T \cdot \nabla \mathbf{N} \, dy \, dz, \tag{15}$$

$$\mathbf{L}_2 = \int_{R_2} \mathbf{N}^T \mathbf{N} \, dy \, dz, \tag{16}$$

$$\mathbf{L}_3 = \int_{R_3} \mathbf{N}^T \mathbf{N} \, dy \, dz, \tag{17}$$

$$\mathbf{L}_{p_2} = \int_{S_{p_2}} \mathbf{N}^T \mathbf{N} \, dy \, dz, \tag{18}$$

$$\mathbf{L}_{p_3} = \int_{S_{p_3}} \mathbf{N}^T \mathbf{N} \, dy \, dz. \tag{19}$$

Here, vectors $\boldsymbol{\Psi}_{p_2}$ and $\boldsymbol{\Psi}_{p_3}$ hold values of $\Psi(y,z)$ on the perforated pipe and S_{p_2} and S_{p_3} denote the surface of the perforated pipe lying in regions R_2 and R_3, respectively.

Eq. (10) is solved for n_r incident and n_r reflected eigenvalues and their associated eigenvectors. Numerical mode matching proceeds by enforcing two matching conditions over the inlet and outlet planes (A and B). The first condition is continuity of pressure and here the incident eigenfunction in region R_1 is chosen as a weighting function, which yields

$$\int_{R_1} p'_1 \Phi_i^n(y,z) \, dR_1 = \int_{R_2} p'_2 \Phi_i^n(y,z) \, dR_2, \tag{20}$$

over plane A, and

$$\int_{R_2} p'_2 \Phi_i^n(y,z)\,\mathrm{d}R_2 = \int_{R_4} p'_4 \Phi_i^n(y,z)\,\mathrm{d}R_4, \tag{21}$$

over plane B. The second matching condition is a kinematic condition, which is chosen here to be the same as that used by Kirby and Denia [5]. Accordingly, the incident eigenfunction in region R_c is chosen as the weighting function and this yields

$$[1 - M\lambda^n]^{-Q}\int_{R_1}\frac{\partial p'_1}{\partial x}\Psi_i^n(y,z)\,\mathrm{d}R_1 = Y\int_{R_c}\frac{\partial p'_c}{\partial x}\Psi_i^n(y,z)\,\mathrm{d}R_c \tag{22}$$

for plane A, and

$$Y\int_{R_c}\frac{\partial p'_c}{\partial x}\Psi_i^n(y,z)\,\mathrm{d}R_c = [1 - M\lambda^n]^{-Q}\int_{R_4}\frac{\partial p'_4}{\partial x}\Psi_i^n(y,z)\,\mathrm{d}R_4 \tag{23}$$

for plane B. Here

$$Y = \left\{ \begin{array}{ll} [1 - Mk^n]^{-Q} & 0 \leqslant r \leqslant r_1 \\ \tilde{\rho} & r_1 \leqslant r \leqslant r_2 \end{array} \right\}, \tag{24}$$

and $\tilde{\rho} = \rho(\omega)/\rho_0$, where $\rho(\omega)$ is the effective (complex) density of the porous material. Eqs. (20)–(23) represent four coupled equations which may be re-written as

$$A^n I_{11_r}^{mn} - B^n I_{C1_i}^{mn} - \tilde{C}^n \mathrm{e}^{\mathrm{i}k_0 k_r^n L} I_{C1_r}^{mn} = -F^0 I_{11_i}^{m0}, \tag{25}$$

$$A^n\frac{\lambda_r^n}{[1 - M\lambda_r^n]^Q}I_{1C_r}^{mn} - B^n k_i^n I_{CC_i}^{mn} - \tilde{C}^n k_r^n \mathrm{e}^{\mathrm{i}k_0 k_r^n L}I_{CC_r}^{mn} = -F^0\frac{\lambda_i^0}{[1 - M\lambda_i^0]^Q}I_{1C_i}^{m0}, \tag{26}$$

$$B^n \mathrm{e}^{-\mathrm{i}k_0 k_i^n L}I_{C1_i}^{mn} + \tilde{C}^n I_{C1_r}^{mn} - D^n I_{11_i}^{mn} = 0, \tag{27}$$

$$B^n k_i^n \mathrm{e}^{-\mathrm{i}k_0 k_i^n L}I_{CC_i}^{mn} + \tilde{C}^n k_r^n I_{CC_r}^{mn} - D^n\frac{\lambda_i^n}{[1 - M\lambda_i^n]^Q}I_{1C_i}^{mn} = 0, \tag{28}$$

where

$$I_{11_{i,r}}^{mn} = \int_{R_1}\Phi_i^m(y,z)\Phi_{i,r}^n(y,z)\,\mathrm{d}y\,\mathrm{d}z \tag{29}$$

$$I_{C1_{i,r}}^{mn} = I_{1C_{i,r}}^{nm} = \int_{R_1}\Psi_i^m(y,z)\Phi_{i,r}^n(y,z)\,\mathrm{d}y\,\mathrm{d}z, \tag{30}$$

$$I_{CC_{i,r}}^{mn} = [1 - Mk_{i,r}^n]^{-Q}\int_{R_2}\Psi_i^m(y,z)\Psi_{i,r}^n(y,z)\,\mathrm{d}y\,\mathrm{d}z + \tilde{\rho}^{-1}\int_{R_3}\Psi_i^m(y,z)\Psi_{i,r}^n(y,z)\,\mathrm{d}y\,\mathrm{d}z, \tag{31}$$

and $\tilde{C}^n = C^n \mathrm{e}^{-\mathrm{i}k_0 k_r^n L}$, for a silencer of length L. The integrals in Eqs. (29)–(31) are carried out numerically after truncating the sums in the inlet and outlet pipes at m_1 and m_4, respectively. Eqs. (25)–(28) are then solved simultaneously for the unknown modal amplitudes after setting $F^0 = 1$, $F^n = 0$ for $n > 0$, and $E^n = 0$ for all n. For plane wave propagation in the inlet and outlet pipes, the silencer TL may then readily be obtained from

$$TL = -20\log_{10}|D^0|. \tag{32}$$

2.2.1. Four pole representation

In the paper by Kirby and Denia [5] expressions are provided for the four poles of a dissipative silencer. These expressions are incorrect. Instead one must solve the systems of equations twice with different axial boundary conditions [25]. The general four pole transfer matrix (for plane wave propagation in the inlet/outlet pipes) is given as

$$\left\{ \begin{array}{c} p'_1(x) \\ u'_1(x) \end{array} \right\} = \left[\begin{array}{cc} T_{11} & T_{12} \\ T_{21} & T_{22} \end{array} \right]\left\{ \begin{array}{c} p'_4(x') \\ u'_4(x') \end{array} \right\}. \tag{33}$$

This system is solved by: (i) setting $p'_4(x') = 0$, which gives $T_{12} = p'_1(x)/u'_4(x')$ and $T_{22} = u'_1(x)/u'_4(x')$ and (ii) setting $u'_4(x') = 0$, which gives $T_{11} = p'_1(x)/p'_4(x')$ and $T_{21} = u_1(x)/p'_4(x')$. It is convenient here to choose $x = x' = 0$ so that the four

pole transfer matrix is coincident with silencer planes A and B. For (i) this gives $D_{(i)}^0 + E_{(i)}^0 = 0$, and

$$T_{12} = \frac{1 + A_{(i)}^0}{D_{(i)}^0 - E_{(i)}^0} Z, \tag{34a}$$

and

$$T_{22} = \frac{1 - A_{(i)}^0}{D_{(i)}^0 - E_{(i)}^0}. \tag{34b}$$

For (ii) $D_{(ii)}^0 - E_{(ii)}^0 = 0$ and

$$T_{11} = \frac{1 + A_{(ii)}^0}{D_{(ii)}^0 + E_{(ii)}^0}, \tag{35a}$$

and

$$T_{21} = \frac{1 - A_{(ii)}^0}{Z(D_{(ii)}^0 + E_{(ii)}^0)}. \tag{35b}$$

Here, $Z = \rho_0 c_0$ and the subscripts (i) and (ii) denote the value of the modal coefficient for solutions (i) and (ii), respectively. The silencer TL may then be calculated from

$$TL = 20 \log_{10} |0.5\{T_{11} + T_{12}/Z + T_{21}Z + T_{22}\}|. \tag{36}$$

Note that the choice of $x = x' = 0$ suppresses the influence of higher order modal scattering close to the inlet and outlet planes in regions R_1 and R_4. To include this scattering, one may simply set $x = -L_{in}$, and $x' = L_{out}$ so that the four pole transfer matrix is computed in regions R_1 and R_4, a distance L_{in} and L_{out} from planes A and B, respectively. A study of the effect of suppressing modal scattering at planes A and B is included towards the end of the following section.

2.3. Hybrid numerical method

A hybrid numerical (HFE) method is reported here, which is based on the method of Kirby [22]. This requires a full finite element discretisation of the silencer chamber and so is based on the method of Peat and Rathi [21], although their method is extended here to include a perforated pipe. Note however that the addition of a perforated pipe means that mean flow in the absorbent material is neglected, and in the analysis that follows only an isotropic porous material is considered. Accordingly, the acoustic pressure in the silencer chamber, region R_c, is approximated by

$$p'_c(x,y,z) = \sum_{j=1}^{n_c} N_j(x,y,z) p_{c_j}, \tag{37}$$

where N_j is a global trial (or shape) function for the finite element mesh, p_{c_j} is the value of the acoustic pressure at node j, and n_c is the number of nodes (or degrees of freedom) in region R_c. Expressing Eq. (37) in vector form yields

$$p'_c(x,y,z) = [N_1(x,y,z), N_2(x,y,z), \ldots, N_{n_c}(x,y,z)] \begin{bmatrix} p_{c_1} \\ p_{c_2} \\ p_{c_{n_c}} \end{bmatrix} = \mathbf{N}\mathbf{p}_c. \tag{38}$$

A weighted residual statement of the wave equation for regions R_2 and R_3 may now be formulated. After application of Green's theorem this yields

$$\left[\int_{R_2} [\nabla \mathbf{N}^T \cdot \mathbf{M} \nabla \mathbf{N} + 2ik_0 \mathbf{N}^T \frac{d\mathbf{N}}{dx} - k_0^2 \mathbf{N}^T \mathbf{N}] \, dx \, dy \, dz \right] \mathbf{p}_2 = \int_{S_2} [\mathbf{N}^T \mathbf{M} \nabla p'_2 \cdot \mathbf{n}_2] \, dS_2 \tag{39}$$

for region R_2, and

$$\left[\int_{R_3} [\nabla \mathbf{N}^T \cdot \nabla \mathbf{N} + \Gamma^2 \mathbf{N}^T \mathbf{N}] \, dx \, dy \, dz \right] \mathbf{p}_3 = \int_{S_3} [\mathbf{N}^T \nabla p'_3 \cdot \mathbf{n}_3] \, dS_3 \tag{40}$$

for region R_3. Here, $\mathbf{p}_2$ and $\mathbf{p}_3$ hold the values of acoustic pressure in regions R_2 and R_3, respectively; S_2 and S_3 denote the outer surface of regions R_2 and R_3, respectively, Γ is the propagation constant of the porous material, and

$$\mathbf{M} = \begin{bmatrix} 1 - M^2 & 0 & 0 \\ 0 & 1 & 0 \\ 0 & 0 & 1 \end{bmatrix}.$$

Eqs. (39) and (40) are coupled together using the pressure and kinematic boundary conditions identified in Eqs. (5) and (6). For clarity it is convenient first to separate out the integrals on the right-hand side of Eqs. (39) and (40), and to write

$$\int_{S_2} [\mathbf{N}^T \mathbf{M} \nabla p'_2 \cdot \mathbf{n}_2] \, dS_2 = \int_{S_A} [\mathbf{N}^T \mathbf{M} \nabla p'_2 \cdot \mathbf{n}_2] \, dS_A + \int_{S_B} [\mathbf{N}^T \mathbf{M} \nabla p'_2 \cdot \mathbf{n}_2] \, dS_B$$
$$+ \int_{S_{p_2}} [\mathbf{N}^T \mathbf{M} \nabla p'_2 \cdot \mathbf{n}_e] \, dS_{p_2}, \tag{41}$$

and

$$\int_{S_3} [\mathbf{N}^T \nabla p'_3 \cdot \mathbf{n}_3] \, dS_3 = \int_{S_{p_3}} [\mathbf{N}^T \nabla p'_3 \cdot \mathbf{n}_3] \, dS_{p_3}, \tag{42}$$

where S_A and S_B denote the surface of planes A and B that lie in region 2, respectively; S_{p_2} and S_{p_3} denote the surface of the perforated pipe that lies in region R_2 and R_3, respectively. Eq. (41) is the key to implementing the HFE method since it is through the integrals over S_A and S_B that the acoustic velocity in the silencer chamber is matched to the velocity in the inlet and outlet pipes. This requires the use of Eqs. (3) and (4), which when substituted into the relevant surface integrals in Eq. (41) yields

$$\int_{S_A} [\mathbf{N}^T \mathbf{M} \nabla p'_2 \cdot \mathbf{n}_2] \, dS_A = i k_0 (1 - M^2) \int_{S_A} \mathbf{N}^T [F^n \lambda_i^n \Phi_i^n + A^n \lambda_r^n \Phi_r^n] \, dS_A, \tag{43}$$

and

$$\int_{S_B} [\mathbf{N}^T \mathbf{M} \nabla p'_2 \cdot \mathbf{n}_2] \, dS_B = -i k_0 (1 - M^2) \int_{S_B} \mathbf{N}^T [D^n \lambda_i^n \Phi_i^n + E^n \lambda_r^n \Phi_r^n] \, dS_B. \tag{44}$$

Note that the summations have been removed here for clarity. It is convenient to re-write these integrals in matrix form, to give

$$\int_{S_A} [\mathbf{N}^T \mathbf{M} \nabla p'_2 \cdot \mathbf{n}_2] \, dS_A = \mathbf{Q}_i^T \mathbf{F} + \mathbf{Q}_r^T \mathbf{A}, \tag{45}$$

and

$$\int_{S_B} [\mathbf{N}^T \mathbf{M} \nabla p'_2 \cdot \mathbf{n}_2] \, dS_B = -\mathbf{R}_i^T \mathbf{D} + \mathbf{R}_r^T \mathbf{E}, \tag{46}$$

where

$$\mathbf{Q}_{i,r} = i k_0 (1 - M^2) \sum_{m=0}^{m_1} \lambda_{i,r}^m \int_{S_A} \Phi^m \mathbf{N}^T \, dS_A, \tag{47}$$

and

$$\mathbf{R}_{i,r} = i k_0 (1 - M^2) \sum_{m=0}^{m_4} \lambda_{i,r}^m \int_{S_B} \Phi^m \mathbf{N}^T \, dS_B. \tag{48}$$

Here, m_1 and m_4 are the number of modes in regions R_1 and R_4, respectively. Note also that $\Phi_i = \Phi_r = \Phi$. The remaining surface integrals in Eqs. (41) and (42) are re-written using the boundary conditions for the perforated pipe given by Eqs. (5) and (6), to give

$$\int_{S_{p_2}} [\mathbf{N}^T \mathbf{M} \nabla p'_2 \cdot \mathbf{n}_2] \, dS_{p_2} = \frac{i k_0}{\zeta} \int_{S_{p_2}} \mathbf{N}^T \left[1 - i \frac{M}{k_0} \frac{\partial}{\partial x} \right]^Q [p'_{p_3} - p'_{p_2}] \, dS_{p_2}, \tag{49}$$

and

$$\int_{S_{p_3}} [\mathbf{N}^T \nabla p'_3 \cdot \mathbf{n}_3] \, dS_{p_3} = -\frac{i k_0}{\zeta} \frac{\rho(\omega)}{\rho_0} \int_{S_{p_3}} \mathbf{N}^T [p'_{p_3} - p'_{p_2}] \, dS_{p_3}. \tag{50}$$

Here, p'_{p_3} and p'_{p_2} denote the acoustic pressure on the perforated pipe in regions R_2 and R_3, respectively. The right-hand side of Eq. (49) contains a second order derivative if $Q = 2$, this may be eliminated by integration, to give

$$\int_{S_{p_2}} [\mathbf{N}^T \mathbf{M} \nabla p'_2 \cdot \mathbf{n}_2] \, dS_{p_2} = \frac{i k_0}{\zeta} \left\{ \int_{S_{p_2}} \left[\mathbf{N}^T \mathbf{N} + (i Q M / k_0) \mathbf{N}^T \frac{d\mathbf{N}}{dx} + \{(Q - 1) M^2 / k_0^2\} \frac{d\mathbf{N}^T}{dx} \frac{d\mathbf{N}}{dx} \right] dS_{p_2} \right\}$$
$$\times [\mathbf{p}_{p_3} - \mathbf{p}_{p_2}] - (Q - 1) \frac{i M^2}{\zeta k_0} \left\{ \int_{S_{c_2}} \mathbf{N}^T \frac{d\mathbf{N}}{dx} \, dS_{c_2} \right\} [\mathbf{p}_{p_3} - \mathbf{p}_{p_2}], \tag{51}$$

where the vectors $\mathbf{p}_{p_2}$ and $\mathbf{p}_{p_3}$ hold the values of acoustic pressure on the perforated pipe in regions R_2 and R_3, respectively, and S_{c_2} represents a pair of circuits at $r = r_1$ on planes A and B. Eqs. (50) and (51) may now be written in matrix

form, to give

$$\int_{S_{p_2}} [\mathbf{N}^T \mathbf{M} \nabla p_2' \cdot \mathbf{n}_2] \, dS_{p_2} = [\mathbf{V}_2 - \mathbf{W}_2][\mathbf{p}_{p_3} - \mathbf{p}_{p_2}], \tag{52}$$

and

$$\int_{S_{p_3}} [\mathbf{N}^T \nabla p_3' \cdot \mathbf{n}_3] \, dS_{p_3} = \mathbf{V}_3 [\mathbf{p}_{p_3} - \mathbf{p}_{p_2}], \tag{53}$$

where

$$\mathbf{V}_2 = \frac{ik_0}{\zeta} \int_{S_{p_2}} \left[\mathbf{N}^T \mathbf{N} + (iQM/k_0) \mathbf{N}^T \frac{d\mathbf{N}}{dx} + \{(Q-1)M^2/k_0^2\} \frac{d\mathbf{N}^T}{dx} \frac{d\mathbf{N}}{dx} \right] dS_{p_2}, \tag{54}$$

$$\mathbf{V}_3 = \frac{ik_0}{\zeta} \frac{\rho(\omega)}{\rho_0} \int_{S_{p_3}} \mathbf{N}^T \mathbf{N} \, dS_{p_3}, \tag{55}$$

and

$$\mathbf{W}_2 = (Q-1) \frac{iM^2}{\zeta k_0} \int_{S_{c_2}} \mathbf{N}^T \frac{d\mathbf{N}}{dx} \, dS_{c_2}. \tag{56}$$

Finally, Eqs. (39) and (40) are re-written using matrix notation and then combined to give

$$\mathbf{G}\mathbf{p}_c - \mathbf{Q}_r^T \mathbf{A} + \mathbf{R}_i^T \mathbf{D} + \mathbf{R}_r^T \mathbf{E} = \mathbf{Q}_i^T \mathbf{F}. \tag{57}$$

Here,

$$\mathbf{G}\mathbf{p}_c = \mathbf{K}_2 \mathbf{p}_2 + \mathbf{K}_3 \mathbf{p}_3 - [\mathbf{V}_2 - \mathbf{V}_3 - \mathbf{W}_2]\{\mathbf{p}_{p_3} - \mathbf{p}_{p_2}\}, \tag{58}$$

$$\mathbf{K}_2 = \int_{R_2} [\nabla \mathbf{N}^T \cdot \mathbf{M} \nabla \mathbf{N} + 2ik_0 \mathbf{N}^T \frac{d\mathbf{N}}{dx} - k_0^2 \mathbf{N}^T \mathbf{N}] \, dx \, dy \, dz, \tag{59}$$

and

$$\mathbf{K}_3 = \int_{R_3} [\nabla \mathbf{N}^T \cdot \nabla \mathbf{N} + \Gamma^2 \mathbf{N}^T \mathbf{N}] \, dx \, dy \, dz. \tag{60}$$

Eq. (57) matches the acoustic velocity in the silencer chamber to that in the inlet and outlet pipes; however, before the problem can be solved a further matching condition is required and here continuity of pressure is enforced separately over planes *A* and *B*. For plane *A*, this gives

$$\sum_{n=0}^{\infty} F^n \Phi_i^n + \sum_{n=0}^{\infty} A^n \Phi_r^n = \mathbf{p}_{2_A}, \tag{61}$$

and for plane *B*

$$\sum_{n=0}^{\infty} D^n \Phi_i^n + \sum_{n=0}^{\infty} E^n \Phi_r^n = \mathbf{p}_{2_B}. \tag{62}$$

Here, $\mathbf{p}_{2_A}$ and $\mathbf{p}_{2_B}$ hold values of the acoustic pressure in region R_2 that lies on S_A and S_B, respectively. It was noted by Astley [23] that in order to obtain a final system matrix that is symmetrical it is necessary to weight each pressure condition using the velocity in the inlet/outlet pipes. Accordingly, for plane *A* the reflected velocity in region R_1 is used, and for plane *B* the incident velocity in region R_4 is used. This then gives

$$\mathbf{M}_1 \mathbf{F} + \mathbf{M}_1 \mathbf{A} - \mathbf{Q}_r \mathbf{p}_{2_A} = \mathbf{0}, \tag{63}$$

and

$$\mathbf{M}_2 \mathbf{D} + \mathbf{M}_2 \mathbf{E} - \mathbf{R}_i \mathbf{p}_{2_B} = \mathbf{0}, \tag{64}$$

where

$$\mathbf{M}_1 = ik_0(1 - M^2) \sum_{m=0}^{m_1} \sum_{n=0}^{m_1} \lambda_r^m \int_{S_A} \Phi^m \Phi^n \, dS_A, \tag{65}$$

and

$$\mathbf{M}_2 = ik_0(1 - M^2) \sum_{m=0}^{m_4} \sum_{n=0}^{m_4} \lambda_i^m \int_{S_B} \Phi^m \Phi^n \, dS_B. \tag{66}$$

Eqs. (57), (63) and (64) are now solved to find the unknown pressures in the silencer chamber and the modal amplitudes in the inlet and outlet pipes. To combine these equations, it is convenient first to write

$$\mathbf{G}\mathbf{p}_c = \begin{bmatrix} \mathbf{G}_{11} & \mathbf{G}_{1e} & \mathbf{G}_{13} \\ \mathbf{G}_{e1} & \mathbf{G}_{ee} & \mathbf{G}_{e3} \\ \mathbf{G}_{31} & \mathbf{G}_{3e} & \mathbf{G}_{33} \end{bmatrix} \begin{Bmatrix} \mathbf{p}_{2A} \\ \mathbf{p}_{ce} \\ \mathbf{p}_{2B} \end{Bmatrix}, \tag{67}$$

where matrix $\mathbf{G}_{mn}$ has order $n_m \times n_n$. Here, n_1 and n_3 denote the number of nodes on S_A and S_B, respectively (where, $m_1 \leqslant n_1$, and $m_4 \leqslant n_3$); n_c is the number of nodes in region R_c, and n_e is the number of nodes that lie in region 2, but do not lie on S_A and S_B (so that $n_e = n_c - n_1 - n_3$). The values for pressure at those nodes in region R_c that do not lie on S_A and S_B are held in matrix $\mathbf{p}_{ce}$. To solve the problem it is necessary to ascribe the axial boundary conditions in the inlet and outlet pipes; to find the silencer TL it is easiest here simply to assume plane wave conditions in the inlet and outlet pipe and to set $F^0 = 1$, $F^n = 0$ for $n > 0$, and $E^n = 0$ for all n. This then gives

$$\begin{bmatrix} \mathbf{M}_1 & -\mathbf{Q}_r & \mathbf{0} & \mathbf{0} & \mathbf{0} \\ -\mathbf{Q}_r^T & \mathbf{G}_{11} & \mathbf{G}_{1e} & \mathbf{G}_{13} & \mathbf{0} \\ \mathbf{0} & \mathbf{G}_{e1} & \mathbf{G}_{ee} & \mathbf{G}_{e3} & \mathbf{0} \\ \mathbf{0} & \mathbf{G}_{31} & \mathbf{G}_{3e} & \mathbf{G}_{33} & \mathbf{R}_i^T \\ \mathbf{0} & \mathbf{0} & \mathbf{0} & \mathbf{R}_i & -\mathbf{M}_2 \end{bmatrix} \begin{bmatrix} \mathbf{A} \\ \mathbf{P}_{2A} \\ \mathbf{p}_{ce} \\ \mathbf{P}_{2B} \\ \mathbf{D} \end{bmatrix} = \begin{bmatrix} -\tilde{\mathbf{M}}_1 \\ \tilde{\mathbf{Q}}_i^T \\ \mathbf{0} \\ \mathbf{0} \\ \mathbf{0} \end{bmatrix}, \tag{68}$$

where

$$\tilde{\mathbf{M}}_1 = ik_0(1 - M^2) \sum_{m=0}^{m_1} \lambda_r^m \int_{S_A} \Phi^m \, dS_A, \tag{69}$$

and

$$\tilde{\mathbf{Q}}_i = ik_0(1 - M^2) \sum_{m=0}^{m_1} \lambda_i^m \int_{S_A} \Phi^m \, dS_A. \tag{70}$$

The silencer TL may then readily be computed using Eq. (32). Alternatively, it is straightforward to solve for the silencer four poles using the method outlined in Section 2.2.1. Here, it is necessary to solve the problem twice: (i) setting $p_4' = 0$ and (ii) setting $u_4' = 0$. In general this may be written as

$$\begin{bmatrix} \mathbf{M}_1 & -\mathbf{Q}_r & \mathbf{0} & \mathbf{0} & \mathbf{0} & \mathbf{0} \\ -\mathbf{Q}_r^T & \mathbf{G}_{11} & \mathbf{G}_{1e} & \mathbf{G}_{13} & \mathbf{0} & \mathbf{0} \\ \mathbf{0} & \mathbf{G}_{e1} & \mathbf{G}_{ee} & \mathbf{G}_{e3} & \mathbf{0} & \mathbf{0} \\ \mathbf{0} & \mathbf{G}_{31} & \mathbf{G}_{3e} & \mathbf{G}_{33} & \mathbf{R}_i^T & \mathbf{R}_r^T \\ \mathbf{0} & \mathbf{0} & \mathbf{0} & \mathbf{R}_i & -\mathbf{M}_2 & -\mathbf{M}_2 \\ \mathbf{0} & \mathbf{0} & \mathbf{0} & \mathbf{0} & \mathbf{I} & \pm\mathbf{I} \end{bmatrix} \begin{bmatrix} \mathbf{A} \\ \mathbf{P}_{2A} \\ \mathbf{P}_{ce} \\ \mathbf{P}_{2B} \\ \mathbf{D} \\ \mathbf{E} \end{bmatrix} = \begin{bmatrix} -\tilde{\mathbf{M}}_1 \\ \tilde{\mathbf{Q}}_i^T \\ \mathbf{0} \\ \mathbf{0} \\ \mathbf{0} \\ \mathbf{0} \end{bmatrix}, \tag{71}$$

with the positive sign used for solution (i) and the negative sign for solution (ii). The silencer four poles may then be obtained from Eqs. (34) and (35). Note that by enforcing the axial matching conditions over the inlet and outlet planes of the silencer modal scattering close to these planes (in regions R_1 and R_4) is suppressed when computing the four poles. This may be avoided by moving planes A and B into regions R_1 and R_4, although this will be at the expense of extending the finite element mesh. Alternatively, one could add in lengths L_{in} and L_{out} in the four pole formulation of Section 2.2.1, which would incur no additional computational expenditure. However, for automotive silencers very little additional energy is likely to be dissipated through the scattering of higher order modes in regions R_1 and R_4. For example, for Silencers 1–3 the addition of inlet and outlet mesh extensions delivers an average change in transmission loss of 0.2 percent (with a maximum of 0.5 percent) when compared to computations that omit the mesh extensions. Accordingly, it is justifiable, at least for the automotive silencers studied here, to keep planes A and B coincident with the inlet and outlet planes of the silencer.

3. Results and discussion

The accuracy and computational efficiency of the four different modelling approaches detailed in Section 2 are investigated here for three circular dissipative silencers. Results will also be presented for two silencers with elliptical cross-sections in view of the change in matching conditions described in Section 2.2. The dimensions of each silencer are listed in Table 1, where the outer radius of the circular silencers is denoted by r_2 and the elliptical silencers have dimensions $a \times b$ where a is the major axis and b is the minor axis. Here, Silencers 1 and 2 have been chosen to match two of the silencers studied by Kirby and Denia [5]; Silencer 3 was studied by Selamet et al. [7] and is included because of a low

Table 1
Dimensions and material parameters for dissipative silencers.

Silencer	Length L (mm)	r_1 (mm)	r_2 (mm)	Absorbent	Θ (Pa s/m^2)	σ
1	315	37	76.2	E glass	30,716	0.263
2	330	37	101.6	E glass	30,716	0.263
3	257.2	24.5	82.2	Fibrous material	4896	0.08
4	350	37	110×60[a]	Basalt wool	13,813	0.263
5	450	37	95×50[a]	E glass	30,716	0.263

[a] Elliptical silencers have dimension $a \times b$, where a is the major axis and b is the minor axis.

perforated pipe porosity; Silencers 4 and 5 are identical to those studied by Kirby [15]. All the calculations that follow assume that mean flow with a Mach number of $M = 0.15$ is present in the airway.

The bulk acoustic properties of the materials contained within each silencer are defined here using Delany and Bazley coefficients, where

$$\Gamma = a_1 \xi^{-a_2} + \text{i}[1 + a_3 \xi^{-a_4}], \tag{72}$$

and

$$\tilde{\rho} = -\Gamma[a_5 \xi^{-a_6} + \text{i}(1 + a_7 \xi^{-a_8})]. \tag{73}$$

Here, the constants $a_1, \ldots, a_8$ are Delany and Bazley coefficients that must be measured for each absorbing material, ξ is the non-dimensional frequency parameter given by $\xi = \rho_0 f / \Theta$ and Θ is the material flow resistivity. Values of the Delany and Bazley constants for E Glass and Basalt wool can be found in Ref. [15], and for Silencer 3 these values can be found in Ref. [7]. A low frequency correction, discussed in detail by Kirby [2,15] is also adopted here, but only for Silencers 1, 2, 4 and 5; this correction is omitted from Silencer 3 in order to remain consistent with the material specification in Ref. [7]. For the perforated pipe the normalised impedance ζ is given by [5]

$$\zeta = [\zeta' + \text{i}0.425k_0 d(\tilde{\rho} - 1)F(\sigma)]/\sigma, \tag{74}$$

where

$$F(\sigma) = 1 - 1.06\sigma^{0.5} + 0.17\sigma^{1.5}. \tag{75}$$

Here, d is the hole diameter, σ is the open area porosity and ζ' is the orifice impedance measured in the absence of an absorbing material. Values for ζ' were measured by Kirby and Cummings [26] and this data is adopted here with $d = 3.5$ mm and the hole thickness $t = 1$ mm for Silencers 1, 2, 4 and 5, for Silencer 3 $d = 2.49$ mm and $t = 0.9$ mm [7]. For a mean flow Mach number of $M = 0.15$ a friction velocity of $u_* = 2.56$ m/s is used for the impedance calculations [26].

The focus of this paper is on investigating the relative accuracy and computational efficiency of four alternative modelling methodologies. Silencer design normally focuses on computing overall silencer performance, which is usually quantified in terms of the silencer TL. Accordingly, the performance of each modelling approach will be judged in terms of the TL predictions and this will be computed without recourse to finding the silencer four-poles. The analysis of each method will begin by examining the convergence of the AMM, NMM and HFE methods. Here, the AMM predictions will follow exactly the method reported by Kirby and Denia [5]. For the NMM method axisymmetry is assumed so that for circular silencers a one-dimensional (y plane) transverse finite element mesh is necessary and here three noded isoparametric line elements are used; for the elliptical silencers a two-dimensional (y and z plane) transverse finite element mesh is necessary and here six noded isoparametric triangular and eight noded isoparametric quadrilateral elements are used. For the HFE method, symmetry allows a two-dimensional cross section to be studied for the circular silencers (x and y plane) and here eight noded quadrilateral elements are used. Furthermore, the inclusion of a perforated pipe in the NMM and HFE models is achieved by adding a node on either side of the perforated pipe, noting that the perforated pipe is treated as an infinitely thin surface in the model and so each adjacent node has an identical location. The analysis of convergence is restricted here to the AMM, NMM and HFE methods because the APW approach does not include an iterative solution and so "convergence" is not defined for this method.

3.1. Circular dissipative silencers

In Figs. 2–4, the convergence of the TL predictions for each method is shown for a frequency of 2 kHz. This frequency has been chosen because it represents an upper limit of the frequency range of interest and so represents a stringent test on convergence. In each figure the relative percentage change in the TL prediction (δE) is plotted against the number of degrees of freedom for the model, where

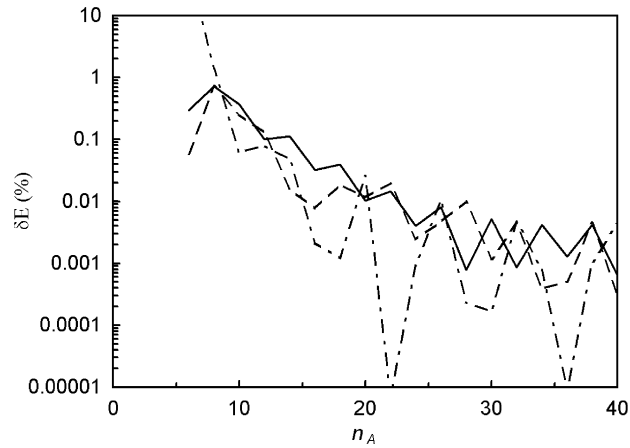$$\delta E_j = 100 \times \frac{[TL_j - TL_{j-1}]}{TL_j}. \tag{76}$$

Fig. 2. Convergence of TL for AMM method at a frequency of 2 kHz: ———, Silencer 1; — — —, Silencer 2; and —·—·—, Silencer 3.
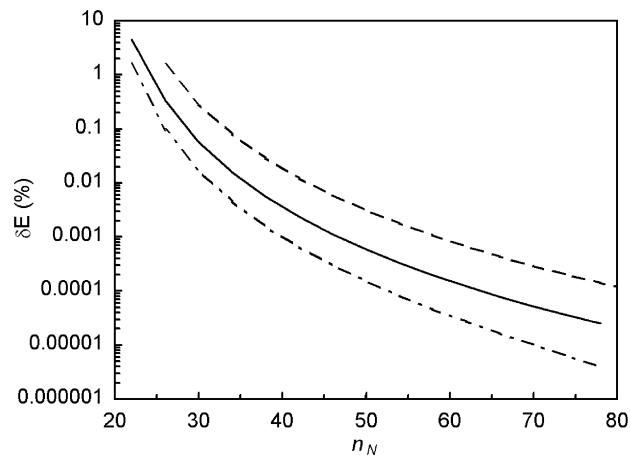

Fig. 3. Convergence of TL for NMM method at a frequency of 2 kHz: ———, Silencer 1; — — —, Silencer 2; and —·—·—, Silencer 3.
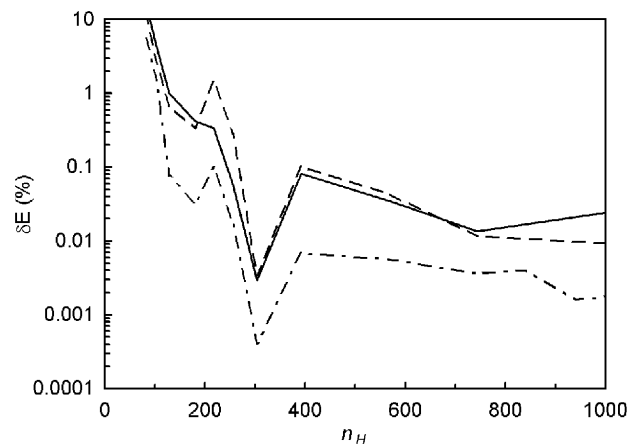

Fig. 4. Convergence of TL for HFE method at a frequency of 2 kHz: ———, Silencer 1; — — —, Silencer 2; and —·—·—, Silencer 3.

Here, δE tracks the percentage change in the TL computation j, when compared to the previous computation $j-1$, so that convergence is achieved when $\delta E \to 0$. Note that as j increases, the number of degrees of freedom in the model is increased; however, in order to properly track convergence it is important to use small increments in the number of degrees of

freedom, n_N and n_H, or the number of modes n_A. For the AMM method n_A denotes the size of the overall system of equations, with $n_A = m_1 + 2m_c + m_4$, where m_1 and m_4 are the number of modes in regions 1 and 4, respectively, and m_c is the number of modes in the silencer chamber (see Ref. [5]). Similarly, for the NMM method, $n_N = m_1 + 2n_s + m_4$ (with $n_s = n_r$), and for the HFE method, $n_H = m_1 + n_c + m_4$.

A comparison between Figs. 2, 3 and 4 indicates that the convergence of the NMM method is much more stable than the AMM and HFE methods. Here, the convergence of the AMM method is rather erratic, although the general trend is similar to that seen for the NMM method. The HFE method also displays rather erratic convergence although achieving smooth convergence for this model is more difficult because one must modify a two-dimensional finite element mesh, which can lead to step changes in accuracy as, say, an extra transverse element is added over the length of the silencer. In contrast, the NMM method exhibits very good convergence and attains low values of δE much faster than the other two methods. However, it should be noted that all three methods converge to values of $\delta E < 0.1$ relatively quickly and, once this limit has been achieved, this level of accuracy is generally maintained. Furthermore, convergence to values of $\delta E < 0.1$ generally equates to convergence in TL predictions to at least one decimal place. This is significant, as practical silencer design is not normally interested in delivering predictions to levels of accuracy greater than one decimal place, especially as one cannot measure TL to this degree of accuracy. Accordingly, convergence to $\delta E = 0.1$ should be viewed as sufficient for most practical uses of the models presented here.

In Figs. 2–4 the number of degrees of freedom required to achieve a given level of convergence is normally much higher for the HFE method when compared to the two mode matching methods. This is to be expected because the AMM and NMM methods utilise the uniform geometry of the silencer section; however, the respective values for n_A, n_N and n_H do not necessarily provide a reliable guide to the relative speed of each method. To investigate this further, values of δE are plotted against the time taken (in seconds) to generate each TL computation in Figs. 5–7, for Silencers 1, 2 and 3 at a frequency of 2 kHz. Here, the APW method has again been omitted, not only because convergence is not defined for this method but also because the predictions are almost instantaneous. For example, after averaging the time taken to compute a large number of frequency calculations, the approximate time to deliver one frequency calculation was estimated to be $t = 0.0005$ s, which is far quicker than the other methods. Of course, this should be no surprise given the nature of the APW method; however, it is the accuracy of this method that is of more interest and this will be reviewed later on in this section. Thus, the focus in Figs. 5–7 is on the rates of convergence of the three other methods and here the relative speed of each method may be compared against one another. The values generated in Figs. 5–7 were computed on a Pentium 4, 3.6 GHz machine with 1 GB of RAM and the values quoted for a single frequency were obtained by running multiple frequency calculations and taking an average value. It is not surprising that in each of these figures the time taken to compute a new TL value increases as the number of degrees of freedom increases. Figs. 5–7 are, however, interesting in that they show the AMM method performing relatively poorly when compared to the two numerical methods. Clearly, the NMM is very quick when compared to the AMM and HFE methods and low values of δE are achieved with very little computational effort. Conversely, the AMM method performs relatively poorly and is at least ten times slower than the NMM method for values of $\delta E \approx 0.1$. The reason for this is that the time taken to solve the NMM equations is largely dictated by the size of the final matrix (n_N), whereas for the AMM method the time taken is dominated by the root finding algorithm. Here, the relatively fast Newton–Raphson method has been used to find the roots (see Ref. [5]), but the number of initial guesses required coupled with an iterative process means that this method is time consuming, especially as one must find both incident and reflected wavenumbers. It is probably possible here to optimise the root finding algorithm further and to improve the speed of this method, but it is unlikely that this will be improved sufficiently to match the speed of the NMM method. These results illustrate the dominance of root finding over the computational speed of the AMM method and so indicate the potential advantages of alternative analytic approaches such as the substructuring method of Albelda et al. [8,11]. Here, if
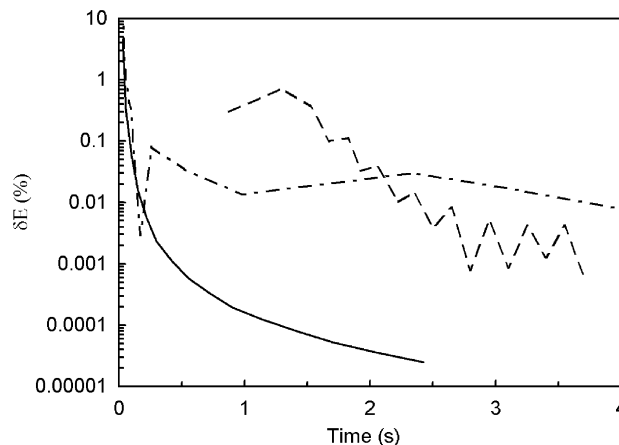

Fig. 5. Rate of convergence for TL of Silencer 1 at a frequency of 2 kHz: ———, NMM method; ————, AMM method; and —·—·—, HFE Method.
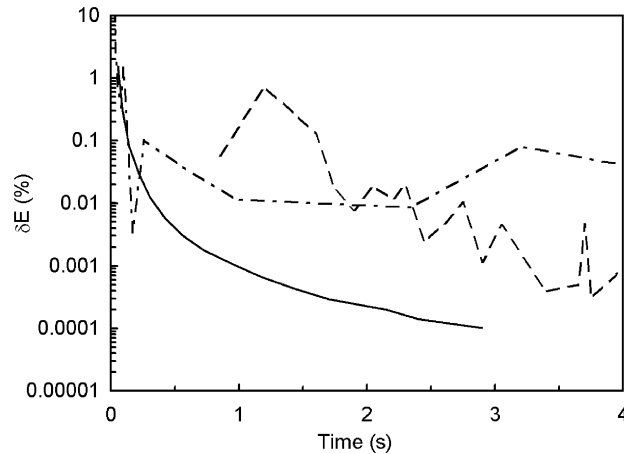
Fig. 6. Rate of convergence for TL of Silencer 2 at a frequency of 2 kHz: ——, NMM method; — — —, AMM method; and —·—·—, HFE Method.
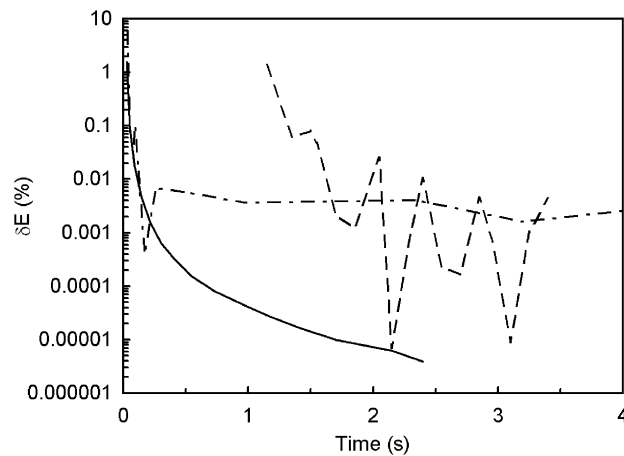

Fig. 7. Rate of convergence for TL of Silencer 3 at a frequency of 2 kHz: ——, NMM method; — — —, AMM method; and —·—·—, HFE Method.

the two subdomain eigenproblems can be solved quickly and one does not require too many modes to obtain a converged solution, then this method should outperform the AMM method. However, firm conclusions await a full reporting of the method, and one doubts that this method would be faster than the NMM method if the number of substructural modes used in the absence of flow [8] are representative of those required when flow is present.

In Figs. 5–7 the speed of convergence of the HFE is seen to be comparable to the NMM method at higher values of δE, but eventually this method slows as higher levels of convergence are sought and eventually the method becomes slower than the AMM method. It is, however, rather surprising to note that the HFE method performs well when compared to the AMM at values of $\delta E \approx 0.1$ and is even comparable in speed to the NMM method. In Fig. 4, the number of degrees of freedom required to deliver convergence to $\delta E \approx 0.1$ is much higher than that seen for the AMM and NMM methods; however, the HFE method delivers a sparse, symmetric and banded matrix, which leads to relatively fast inversion when compared to mode matching methods that invert dense non-symmetric matrices. Accordingly, the results presented here demonstrate that the time taken to invert a small but dense non-symmetric matrix is similar to that taken to invert a much larger but banded symmetric matrix. Therefore, for values of $\delta E \approx 0.1$ the HFE method is capable of computations with a speed comparable to the NMM method but faster than an equivalent analytic method, a point that is often not recognised in the literature. Of course, as one increases values of n_H the time taken to solve the HFE problem increases rapidly, but only at relatively high values of n_H is the HFE method seen to become slower than the AMM method.

The final test for each method is a comparison between the accuracy of the predictions generated. Accuracy will be examined here first by comparing TL predictions converged to two decimal places, and then by comparing predictions converged to $\delta E \approx 0.1$. This allows a comparison between the accuracy that each method is capable of and also the accuracy that may be achieved if one is interested in economising on computational speed. In Tables 2–4, a comparison between TL predictions converged to two decimal places is shown for Silencers 1–3. Here, problems with the accuracy of the APW

Table 2
Transmission loss values for Silencer 1 converged to two decimal places and after optimising for computational speed (in parentheses).

Frequency (Hz)	APW (dB)	AMM (dB)	HFE (dB)	NMM (dB)
50	1.88	1.45 (1.4)	1.43 (1.4)	1.45 (1.5)
100	3.30	2.75 (2.7)	2.73 (2.7)	2.76 (2.8)
250	5.60	5.04 (5.0)	5.03 (5.0)	5.04 (5.0)
500	12.69	11.62 (11.6)	11.62 (11.6)	11.61 (11.6)
750	18.95	17.63 (17.6)	17.62 (17.6)	17.62 (17.6)
1000	23.67	22.30 (22.3)	22.30 (22.3)	22.29 (22.3)
1500	29.23	26.61 (26.6)	26.61 (26.6)	26.61 (26.6)
2000	23.84	27.35 (27.4)	27.34 (27.3)	27.35 (27.4)

Table 3
Transmission loss values for Silencer 2 converged to two decimal places and after optimising for computational speed (in parentheses).

Frequency (Hz)	APW (dB)	AMM (dB)	HFE (dB)	NMM (dB)
50	4.64	3.29 (3.2)	3.29 (3.3)	3.29 (3.3)
100	5.62	4.58 (4.5)	4.60 (4.6)	4.59 (4.6)
250	10.14	8.65 (8.6)	8.71 (8.7)	8.65 (8.7)
500	16.79	14.36 (14.4)	14.41 (14.4)	14.35 (14.4)
750	19.64	17.84 (17.8)	17.84 (17.8)	17.83 (17.8)
1000	20.29	20.29 (20.3)	20.28 (20.3)	20.28 (20.3)
1500	20.53	25.00 (25.0)	25.01 (25.0)	24.99 (25.0)
2000	22.68	29.44 (29.5)	29.45 (29.4)	29.43 (29.4)

Table 4
Transmission loss values for Silencer 3 converged to two decimal places and after optimising for computational speed (in parentheses).

Frequency (Hz)	APW (dB)	AMM (dB)	HFE (dB)	NMM (dB)
50	2.93	3.71 (3.7)	3.73 (3.7)	3.72 (3.7)
100	6.84	6.32 (6.3)	6.37 (6.4)	6.33 (6.3)
250	12.83	9.98 (10.0)	9.97 (10.0)	9.98 (10.0)
500	17.07	14.43 (14.4)	14.43 (14.4)	14.43 (14.4)
750	20.97	19.80 (19.8)	19.80 (19.8)	19.78 (19.8)
1000	23.24	24.79 (24.8)	24.91 (24.9)	24.77 (24.8)
1500	25.66	39.26 (39.3)	39.70 (39.7)	39.28 (39.3)
2000	21.45	24.84 (24.8)	24.86 (24.8)	24.83 (24.8)

method are obvious at higher frequencies as well as for a perforated pipe of low porosity. This supports the observations made by Kirby [2] and indicates that, although the APW method provides instantaneous predictions, the accuracy of these predictions is acceptable only if one is interested in relatively low frequencies, say below 500 Hz. For the other three methods very good agreement between TL predictions is observed over the entire frequency range. This serves to validate the NMM and HFE models in Sections 2.2 and 2.3, respectively. It is interesting also to note the very good agreement between the HFE method and the two mode matching techniques. In the article by Kirby and Denia [5] it was proposed that continuity of displacement should be used for the axial kinematic matching condition over the inlet/outlet planes of the silencer, but only if continuity of displacement was already being used for the transverse kinematic condition over the perforated pipe. Accordingly, the NMM method reported here adopts this suggestion and so matches using the same conditions as those adopted by the AMM method. In contrast, the HFE method described in Section 2.3 uses continuity of displacement over the perforated pipe and (the more usual) continuity of velocity over the silencer inlet/outlet planes. The excellent agreement between each method thus lends support to the observations of Kirby and Denia [5] and suggests that modifying the axial kinematic condition is necessary only when using a modal expansion for the sound pressure field in the silencer section.

Tables 2–4 also contain TL predictions converged to $\delta E \approx 0.1$ (in parentheses). This level of accuracy roughly equates to a TL prediction converged to one decimal place and is therefore designed to record the level of accuracy possible when lowering the solution time. Accordingly, the data in parentheses in Tables 2–4 should be viewed in conjunction with Figs. 5–7. Here, the TL predictions are virtually identical for the AMM, NMM and HFE methods and so, when considering accuracy to only one decimal place, the same predictions are obtained regardless of the method chosen. Therefore, one may chose an appropriate method based on the speed of solution, and an examination of Figs. 5–7 clearly shows that the NMM

is the fastest of the three techniques, and is significantly faster than the AMM method. What is interesting, however, is that the HFE method also outperforms the AMM method and is comparable in speed to the NMM method, at least for the dissipative silencers studied here. Clearly, this result has ramifications when choosing a modelling technique. Here, it is not necessarily the case that a numerical method is always slower than an analytic method. The results presented indicate that the opposite is true if one is only interested in generating TL predictions for automotive silencers to an accuracy of one decimal place, which normally represents an acceptable level of accuracy. Therefore, for simple circular dissipative silencers the NMM method provides a reliable technique that does not depend on mode matching and is significantly faster than an equivalent analytic method; for more complex but axially uniform silencer geometries, such as those which include inlet/outlet extensions, the HFE method is also capable of outperforming the AMM and modifying the finite element mesh to accommodate more complex geometries is very straightforward.

3.2. Elliptical dissipative silencers

The NMM model presented in Section 2.2 is a modified version of the point collocation method of Kirby [15] that includes the new axial kinematic matching condition later suggested by Kirby and Denia [5]. In view of these changes it is appropriate here to revisit those predictions presented in Ref. [15]. Accordingly, predictions are presented in Figs. 8 and 9 for Silencers 4 and 5 (see Table 1). The TL predictions presented in Figs. 8 and 9 are for values of $\delta E \approx 0.1$ and were obtained using $n_S = 74$, $m_1 = m_4 = 1$ and $n_r = 4$. Furthermore, after taking an average of the time taken to compute the TL for a number of different frequencies, the time taken for a single frequency is estimated to be 0.68 s, which compares well with the time taken for circular silencers. It is evident in Figs. 8 and 9 that the agreement between prediction and experiment has improved when compared to the equivalent predictions presented by Kirby [15]; however, the difference is small, which is probably because of the high material flow resistivity used in Silencers 4 and 5 (see Ref. [5] for a fuller discussion on the influence of material flow resistivity on the axial boundary condition). A comparison between prediction and
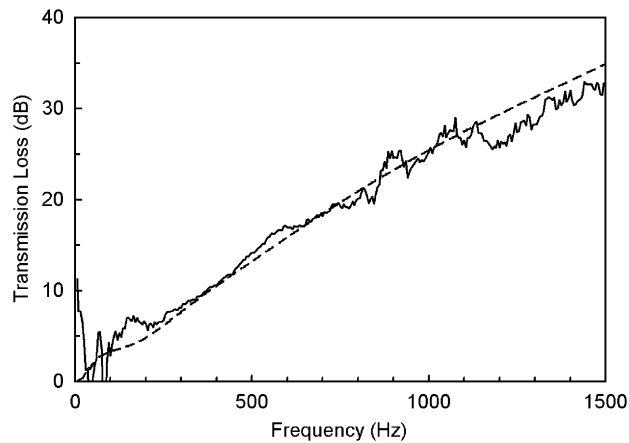

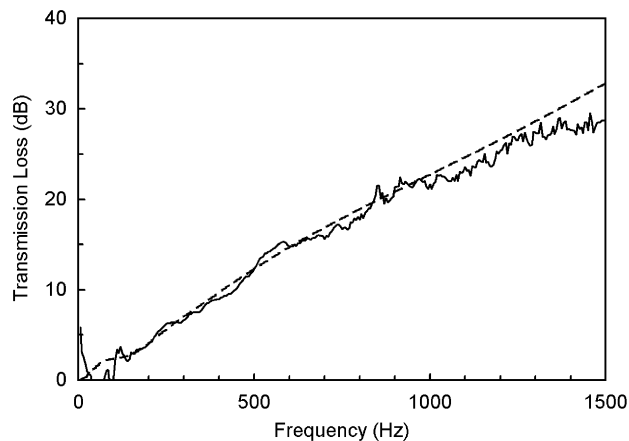**Fig. 8.** TL for Silencer 4: ———, experiment [15] and — — —, NMM predictions.

Fig. 9. TL for Silencer 5: ———, experiment [15] and — — —, NMM predictions.

experiment does, however, demonstrate the accuracy that may be achieved using the NMM method for elliptical silencers, and this may be achieved in a time that is comparable to that achievable when using the AMM for circular silencers.

4. Conclusions

Two numerical and two analytic models are compared here. The analytic models include the plane wave approach of Kirby [2] and the AMM method of Kirby and Denia [5]. Here, the plane wave approach is shown to be inaccurate at higher frequencies, but also when perforated pipes of low porosity are present. Accordingly, in order to be confident of accurate predictions above approximately 500 Hz, it is necessary to include higher order modes in the modelling methodology. The accuracy and speed of the AMM method is then compared to two new numerical models: the point collocation approach of Kirby [15], which is modified in order to implement a numerical version of mode matching, and the finite element approach of Peat and Rathi [21], which is modified to include a perforated pipe and a more efficient hybrid finite element method.

A comparison between the AMM method and the two numerical methods shows excellent agreement between the transmission loss predictions obtained for the three silencers studied here. This then allows one to choose an appropriate modelling technique on the basis of speed and/or flexibility, and here it is shown that the numerical models perform very well when compared to the AMM method. For example, the NMM method is shown to be significantly faster than both the AMM and HFE methods for each of the silencers studied here. This is because the NMM does not require an iterative algorithm to find the roots of the silencer eigenequation (necessary in the AMM method), and the number of modes required to obtain an accurate solution is relatively small. Accordingly, the number of degrees of freedom required in the (transverse) finite element mesh is relatively small for the NMM method, even for an asymmetric cross-section. However, what is perhaps surprising is that the new HFE method also provides relatively fast solutions. Here, if one is interested only in generating transmission loss predictions accurate to one decimal place, then the HFE method is as least as fast as the AMM method, and in most cases faster. This is because, in addition to avoiding the need to use iterative root finding techniques, the HFE method delivers a banded symmetric matrix and this facilitates fast matrix inversion despite the increase in the number of degrees of freedom. Accordingly, predictions can be generated quickly when using the HFE method and the normal assumption in the literature that analytic equals fast, and numerical equals slow, are not necessarily true, at least for automotive dissipative silencers. Therefore, for more complex silencer geometries the flexibility of the HFE method becomes attractive and for silencers that include, say, inlet and outlet extensions, a numerical approach can readily be applied in the knowledge that this will not necessarily be slower than the more usual analytic approach.

It is shown here that automotive dissipative silencers that contain mean flow and a perforated pipe can be modelled accurately and even when using numerical methods these models can run very quickly on a desktop PC. Accordingly, such models can readily be applied in an iterative design environment and from the results presented here, the most efficient technique for a uniform dissipative silencer is a numerical mode matching technique.

References

[1] K.S. Peat, A transfer matrix for an absorption silencer element, *Journal of Sound and Vibration* 146 (1991) 353–360.
[2] R. Kirby, Simplified techniques for predicting the transmission loss of a circular dissipative silencer, *Journal of Sound and Vibration* 243 (2001) 403–426.
[3] A. Cummings, I.-J. Chang, Sound attenuation of a finite length dissipative flow duct silencer with internal mean flow in the absorbent, *Journal of Sound and Vibration* 127 (1988) 1–17.
[4] S.N. Panigrahi, M.L. Munjal, Comparison of various methods for analysing lined circular ducts, *Journal of Sound and Vibration* 285 (2005) 905–923.
[5] R. Kirby, F.D. Denia, Analytic mode matching for a circular dissipative silencer containing mean flow and a perforated pipe, *Journal of the Acoustical Society of America* 122 (2007) 3471–3482.
[6] M.B. Xu, A. Selamet, I.-J. Lee, N.T. Huff, Sound attenuation in dissipative expansion chambers, *Journal of Sound and Vibration* 272 (2004) 1125–1133.
[7] A. Selamet, M.B. Xu, I.-J. Lee, N.T. Huff, Analytical approach for sound attenuation in perforated dissipative silencers, *Journal of the Acoustical Society of America* 115 (2004) 2091–2099.
[8] J. Albelda, F.D. Denia, M.I. Torres, F.J. Fuenmayor, A transversal substructuring mode matching method applied to the acoustic analysis of dissipative mufflers, *Journal of Sound and Vibration* 303 (2007) 614–631.
[9] F.D. Denia, A. Selamet, F.J. Fuenmayor, R. Kirby, Acoustic attenuation performance of perforated dissipative mufflers with empty inlet/outlet extensions, *Journal of Sound and Vibration* 302 (2007) 1000–1017.
[10] R. Kirby, J.B. Lawrie, A point collocation approach to modelling large dissipative silencers, *Journal of Sound and Vibration* 286 (2005) 313–339.
[11] J. Albelda, F.D. Denia, F.J. Fuenmayor, M.J. Martínez, A transversal substructuring modal method for the acoustic analysis of dissipative silencers with mean flow, *Journal of the Acoustical Society of America* 123 (2008) 3534.
[12] R.J. Astley, A. Cummings, N. Sormaz, A finite element scheme for acoustic propagation in flexible-walled ducts with bulk-reacting liners, and comparison with experiment, *Journal of Sound and Vibration* 150 (1991) 119–138.
[13] R. Glav, The point-matching method on dissipative silencers of arbitrary cross-section, *Journal of Sound and Vibration* 189 (1996) 123–135.
[14] R. Glav, The transfer matrix for a dissipative silencer of arbitrary cross-section, *Journal of Sound and Vibration* 236 (2000) 575–594.
[15] R. Kirby, Transmission loss predictions for dissipative silencers of arbitrary cross section in the presence of mean flow, *Journal of the Acoustical Society of America* 114 (2003) 200–209.
[16] S. Bilawchuk, K.R. Fyfe, Comparison and implementation of the various numerical methods used for calculating transmission loss in silencer systems, *Applied Acoustics* 64 (2003) 903–916.
[17] T.W. Wu, P. Zhang, C.Y.R. Cheng, Boundary element analysis of mufflers with an improved method for deriving the four-pole parameters, *Journal of Sound and Vibration* 217 (1998) 767–779.
[18] A. Selamet, I.-J. Lee, N.T. Huff, Acoustic attenuation of hybrid silencers, *Journal of Sound and Vibration* 262 (2003) 509–527.

[19] S.N. Panigrahi, M.L. Munjal, A generalized scheme for analysis of multifarious commercially used mufflers, *Applied Acoustics* 68 (2007) 660–681.
[20] O.Z. Mehdizadeh, M. Paraschivoiu, A three-dimensional finite element approach for predicting the transmission loss in mufflers and silencers with no mean flow, *Applied Acoustics* 66 (2005) 902–918.
[21] K.S. Peat, K.L. Rathi, A finite element analysis of the convected acoustic wave motion in dissipative silencers, *Journal of Sound and Vibration* 184 (1995) 529–545.
[22] R. Kirby, Modeling sound propagation in acoustic waveguides using a hybrid numerical method, *Journal of the Acoustical Society of America* 124 (2008) 1930–1940.
[23] R.J. Astley, FE mode-matching schemes for the exterior Helmholtz problem and their relationship to the FE-DtN approach, *Communications in Numerical Methods in Engineering* 12 (1996) 257–267.
[24] F.D. Denia, L. Baeza, J. Albelda, F.J. Fuenmayor, Acoustic behaviour of elliptical mufflers with single-inlet and double-outlet, *Proceedings of the 10th International Congress on Sound and Vibration*, Stockholm, July 2004, pp. 3287–3294.
[25] K.S. Peat, Evaluation of four-pole parameters for ducts with flow by the finite element method, *Journal of Sound and Vibration* 84 (1982) 389–395.
[26] R. Kirby, A. Cummings, The impedance of perforated plates subjected to grazing mean flow and backed by porous media, *Journal of Sound and Vibration* 217 (1998) 619–636.